Chemical Science

ROYAL SOCIETY OF CHEMISTRY

EDGE ARTICLE

View Article Online
View Journal | View Issue





Cite this: *Chem. Sci.*, 2022, **13**, 2026

All publication charges for this article have been paid for by the Royal Society of Chemistry

Received 17th December 2021
Accepted 22nd January 2022

DOI: 10.1039/d1sc07041j

rsc.li/chemical-science

# Nonspherical anion sequestration by C–H hydrogen bonding†

Saber Mirzaei, Victor M. Espinoza Castro and Raúl Hernández Sánchez *

Macrocyclic arenes laid the foundations of supramolecular chemistry and their study established the fundamentals of noncovalent interactions. Advancing their frontier, here we designed rigidified resorcin[4]arenes that serve as hosts for large nonspherical anions. In one synthetic step, we vary the host's anion affinity properties by more than seven orders of magnitude. This is possible by engineering electropositive aromatic C–H bond donors in an idealized square planar geometry embedded within the host's inner cavity. The hydrogen atom's electropositivity is tuned by introducing fluorine atoms as electron withdrawing groups. These novel macrocycles, termed fluorocages, are engineered to sequester large anions. Indeed, experimental data shows an increase in the anion association constant ($K_a$) as the number of F atoms increase. The observed trend is rationalized by DFT calculations of Hirshfeld Charges (HCs). Most importantly, fluorocages in solution showed weak-to-medium binding affinity for large anions like $[PF_6]^-$ ($10^2 < K_a < 10^4$ $M^{-1}$), and high affinity for $[MeSO_3]^-$ ($K_a > 10^6$).

## Introduction

Macrocyclic arenes are quintessential compounds in the development of host–guest chemistry.[1–5] Guests are usually hosted within the inner cavity of the macrocycle through non-covalent interactions, *e.g.*, hydrogen bonding, π···π stacking, and C–H···π interactions.[6] Among these non-covalent interactions, hydrogen bonding is the strongest one,[7] especially when considering oxygen and nitrogen, where the difference in Pauling electronegativity with hydrogen ($\Delta\chi$) is 1.24 and 0.84,[8] respectively. Lehn *et al.* recognized in 1976 that incorporating hydrogen bonding capabilities (N–H bonds) within cryptands resulted in weak-to-medium affinity for spherical anions (*e.g.*, halides),[9,10] this realization opened the door to "anion coordination chemistry".[11] Later reports demonstrated fluorinated macrocycles hosting fluoride ion purely through C–H···$F^-$ hydrogen bonding,[12] which is remarkable noting that $\Delta\chi$ for C and H is just 0.35. However, due to the relatively weak binding affinities, molecular designs for anion binding based solely on C–H hydrogen bonding were marginalized in supramolecular host–guest chemistry.[13,14] This notion has been challenged, and in the past few decades a range of hosts with remarkable affinities towards spherical anions ($K_a > 10^6$ $M^{-1}$) have been reported by J. L. Sessler,[15–17] P. A. Gale,[18] A. P. Davis,[18–20] B. D. Smith,[20] A. H. Flood,[21–25] V. Sindelar,[26,27] J. Yoon,[28] J. You,[29] M. Pittelkow,[30] H. Jiang,[31] M. Stępień,[32] and others.[33]

Molecular recognition of nonspherical anions have transformed the design of rotaxane assemblies,[34] advanced novel catalytic processes by stabilization of *in situ* generated anions,[35] laid the ground work supporting anion–anion stabilization theories,[36] facilitated ion pair dissociation in battery electrolytes,[37] and provided systems of remarkable selectivity towards the recognition of bifluoride,[38] organophosphates,[39] dicarboxylates,[40] the biologically relevant GTP anion,[41] nitrate,[42,43] and sulfate.[44] Despite these noteworthy advances, hosts capable of binding nonspherical anions with high affinity are rare and usually lack synthetic tunability requiring a complete host redesign to tune binding affinities, therefore efforts to develop hosts for nonspherical anions remains a challenge. Herein, we report a strategy to create novel supramolecular anion cages through a straightforward and versatile synthetic procedure in which we discovered binding preferences for nonspherical anions.

## Results and discussion

### Host–guest design

Fluorocages, as we refer to these supramolecular hosts, were conceived by trying to maximize the host–guest properties of resorcin[*n*]arenes[45] towards anionic species. Note that while their host–guest capabilities for neutral guests are well-established,[6] their anion hosting abilities are not nearly as developed.[46,47] Towards this goal, we designed and synthesized a modular family of resorcin[4]arene-based cages, **1–8** (Scheme 1), all having the same binding cage geometry capable of

*Department of Chemistry, University of Pittsburgh, 219 Parkman Ave., Pittsburgh, Pennsylvania, 15260, USA. E-mail: raulhs@pitt.edu*

† Electronic supplementary information (ESI) available: Experimental methods, $^1H$, $^{13}C$, $^{19}F$, COSY, and titration NMR spectra, crystallographic details, DFT calculations. CCDC 2104069–2104080. For ESI and crystallographic data in CIF or other electronic format see DOI: 10.1039/d1sc07041j

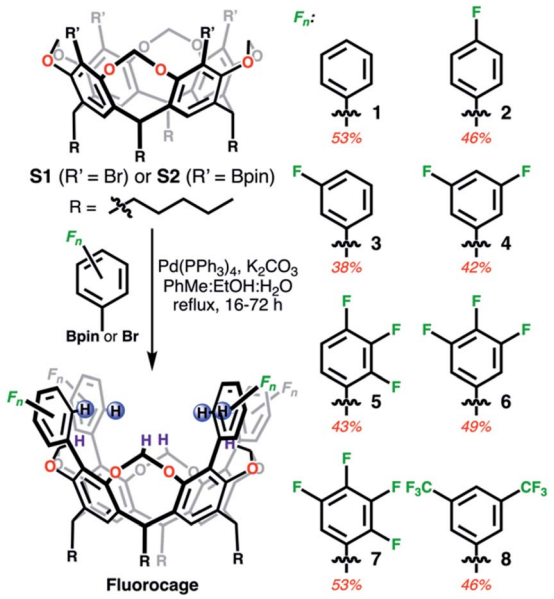


Scheme 1 Synthesis of fluorocages **1–8**.

accommodating large guests, and also able to tune the overall framework to systematically and monotonically increase the anion binding affinity.

### Fluorocages structure

Fluorocages **1–8** were synthesized from **S1** (ref. 48) or **S2** (ref. 49) through Suzuki–Miyaura cross-coupling reactions with the corresponding aromatic flanking unit, $F_n$ as described in Scheme 1, in yields ranging from 38 to 53% (see ESI†). All hosts define a cavity comprised of eight C–H donors, four aromatic colored in blue ($C_{Ar}$–H) and four aliphatic colored in dark purple ($C_{CH_2}$–H). Our hypothesis is that installing electron withdrawing groups (EWGs) on the aromatic flanking units would produce sufficiently high electropositive hydrogen atoms in $C_{Ar}$–H capable of binding anionic species with high affinity. Moreover, fluorocages **1–8** are designed as rigid scaffolds to minimize entropic penalties that may arise from conformational flexibility and host rearrangement upon guest binding.[50,51]

$^1$H, $^{13}$C, and $^{19}$F NMR spectra in $CDCl_3$ of **1–4**, **6**, and **8** reveals their expected ideal $C_{4v}$ molecular symmetry in solution (see ESI†). Fluorocages **5** and **7** display a more complex behavior (Fig. S26–S28 and S32–S34†), however in-depth analysis of their $^1$H NMR spectra corroborates their assignment. High quality crystals for single-crystal X-ray diffraction for **1–8** provided further confirmation of their molecular structure (Fig. 1). Crystals of **1–8** were all obtained by slow evaporation of a MeCN : $CH_2Cl_2$ solution at room temperature. Note that all fluorocage structures display one molecule of MeCN bound within their inner cavity, except **7** which displayed heavy disorder that prevented correct modeling of the MeCN molecule. The molecular structures of **3**, **5**, and **7** displayed rotational disorder around their aromatic flanking units. For example, fluorocage **3** displays in the major occupancy structure three F atoms pointing into the inner cavity while one F atom is pointing away. Nonetheless, this behavior is not manifest in solution, as the NMR data indicates a fully $C_4$-symmetric structure. In contrast, **5** and **7** display solid state major occupancy structures with idealized $C_s$ and $C_{2v}$ point group symmetries, respectively, which is reconciled with their complex solution behavior indicating that rotation around the biaryl moiety is hampered and that all possible rotational isomers coexist in solution, even at 100 °C (Fig. S69 and S71†). Up to six different rotamers are possible for **5** and **7**. DFT calculations at the M06-2X/6-311++G(3df,2p)+CPCM(solvent)//M06-2X/6-31+G(d,p) level of theory, where solvent = $CHCl_3$ or DMSO, showed that these rotamers are relatively close in energy, thus supporting the experimental observations in solution (Tables S2 and S3†).

### Anion affinity towards square planar electropositive cavity

The design and engineering of the electropositive cavity within **1–8** is best exemplified by the hosted MeCN molecule, which has its electronegative N atom residing in the same plane as the

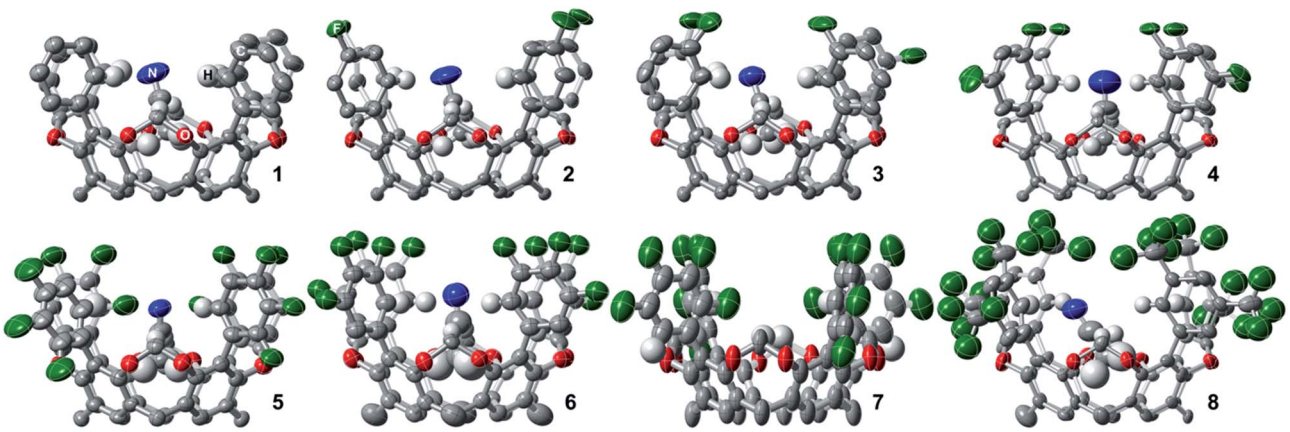


Fig. 1 Molecular crystal structures of fluorocages **1–8**. Thermal ellipsoids are set at 50% probability level (except for **6** which are at 30%). The R groups (*n*-pentyl) and H atoms are omitted for clarity, except those H atoms within the fluorocage's inner cavity. The C, N, O, F, and H atoms are colored grey, blue, red, green, and white, respectively.

Table 1 Anion association constants ($K_a$, $M^{-1}$) of $[PF_6]^-$ and $[MeSO_3]^-$ to fluorocages **1–8**

| Salt | Solvent | **1** | **2** | **3** | **4** | **5** | **6** | **7** | **8** |
|---|---|---|---|---|---|---|---|---|---|
| $[n\text{-}Bu_4N]$ $[PF_6]$ | $CDCl_3$ | 0 | 0 | 0 | 84(12) | 0 | $1.510(1) \times 10^4$ | $1.64(11) \times 10^3$ | 280(15) |
| $[n\text{-}Bu_4N]$ $[MeSO_3]$ | DMSO-$d_6$ | ND[a] | ND[a] | ND[a] | $>10^{6}$[b] | $>10^{6}$[b] | $>10^{6}$[b] | $>10^{6}$[b] | ND[c] |

[a] ND = Not determined. [b] Strong binding that prevents direct titration *via* $^1$H NMR, even at 100 °C the anion remains bound. $10^6$ $M^{-1}$ is taken as the maximum reliable limit for NMR titration experiments.[52] [c] Not soluble in DMSO-$d_6$ even at 100 °C.

cavity's electropositive H atoms (colored in blue in Scheme 1). The average C-to-N distances ($C_{Ar}$–H and $N_{MeCN}$) for all fluorocages is 4.0 ± 0.2 Å [4.0(2) Å (number in parenthesis indicates the estimated standard deviation in the final digit)], while the average C-to-π system centroid ($C_{MeCN}$ and centroid of each aromatic ring comprising the resorcin[4]arene base) is 3.55(4) Å. Anion sequestration was first tested by $^1$H NMR titration experiments adding $[n\text{-}Bu_4N][PF_6]$ to **2–8** in $CDCl_3$ (solvent dielectric constant, $\varepsilon_r = 4.7$) at 20 °C (Table 1 and Fig. S38–S44†). There is negligible affinity for $[PF_6]^-$ by **1–3**, however **4**, **6**, and **8** display weak-to-medium binding peaking at **6** with $K_a$ of $1.510(1) \times 10^4$ $M^{-1}$, while **4** and **8** display $K_a$ of 84(12) and 280(15) $M^{-1}$, respectively. To our surprise, **5** displays no binding of $[PF_6]^-$, while **7** only reaches $K_a = 1.64(11) \times 10^3$ $M^{-1}$, likely as a result of the energetic penalty involved in rearranging their initial conformational distribution. Note that only a few synthetic hosts are known to bind large anions such as $[PF_6]^-$.[22,34,46,53] Overall, the adduct $[PF_6 \subset \mathbf{6}]^-$ demonstrates that the square planar arrangement of electropositive H atoms serves to sequester large anionic species.

Encouraged by the binding results of $[PF_6]^-$, we tested the ability of fluorocage **6** to bind other noncoordinating nonspherical anions. For reference, the large iodide anion, with a thermochemical radii ($r$)[54] of 2.11(19) Å displays a $K_a = 161(19)$ $M^{-1}$ (Fig. S45†); and as the spherical anion shrinks, *e.g.* $Br^-$ ($r =$ 1.90(19) Å), the observed $K_a$ goes to zero (Fig. S46†). Linear $[N_3]^-$ and $[SCN]^-$, bent $[NO_2]^-$, and trigonal planar $[NO_3]^-$ have negligible-to-weak binding affinities (Table 2, Fig. S47–S50†), likely resulting from their size mismatch with the host's cavity. However, strong binding is observed as the anion's size reaches a radius of ~2.2 Å judging from the series $[BF_4]^-$ ($r = 2.05(19)$ Å, Fig. S51†), $[HSO_4]^-$ ($r = 2.21(19)$ Å, Fig. S52†), $[ClO_4]^-$ ($r =$ 2.25(19) Å, Fig. S53†), $[ReO_4]^-$ ($r = 2.27(19)$ Å, Fig. S54†), $[IO_4]^-$ ($r = 2.31(19)$ Å, Fig. S55†), and $[SbF_6]^-$ ($r = 2.52(19)$ Å, Fig. S56†). Note that anion binding affinity decreases by about two orders of magnitude when the anion's size surpass $[PF_6]^-$, as observed in $[SbF_6]^-$ which is only ~4% larger than $[PF_6]^-$. Thus, we establish that the optimum anion's size fitting in the host's cavity must be $2.2 < r < 2.4$ Å. Other nonspherical anions, such as acetate, $[MeCO_2]^-$, also binds to **6** ($K_a = 4.8(3) \times 10^3$ $M^{-1}$, Fig. S57†), however the closely related $[MeSO_3]^-$ binds so strongly to **6** in $CDCl_3$ that its affinity falls beyond the reliable measurable limit *via* $^1$H NMR ($10^6$ $M^{-1}$), see Fig. 2a.[52] Note that a marked downfield complexation-induced chemical shift occurs for protons "*a*" ($\Delta\delta \approx 0.57$ ppm) and "$b_{in}$" ($\Delta\delta \approx 0.69$ ppm) as established for H atoms involved in direct hydrogen bonding with the bound anion (Fig. 2a). In contrast, proton "$b_{out}$" shifts upfield as a result of increased electron density on the C atom (methylene) due to anion binding.[56] We conclude that sulfonate's structure is better poised to interact with the four electropositive H atoms as opposed to the flat structure of carboxylate. Note that *p*-toluenesulfonate, $[p\text{TsO}]^-$, with its much larger organic group, also binds to **6** displaying a $K_a$ of $1.88(4) \times 10^3$ $M^{-1}$, where its *p*-toluene fragment points away from the fluorocage's cavity (Fig. S59 and S60, Table S4†).

Sulfonate anion appears to have the optimum size to fit in the cavity described by the four electropositive H atoms in $C_{Ar}$–H. Intrigued by this observation, we decided to expand our efforts and investigate the binding properties of $[MeSO_3]^-$ towards **1–5** and **7–8** in $CDCl_3$ at 20 °C. Host **1** failed to bind $[MeSO_3]^-$ (Fig. S61†). Fluorocages **2** and **3** displayed binding of $[MeSO_3]^-$ with $K_a$ of 22(4) and 667(38) $M^{-1}$ (Fig. S62 and S63†), respectively, while host **8** exhibited slow exchange[57,58] in the NMR time scale with $K_a \approx 2.5(2) \times 10^3$ $M^{-1}$ (Fig. S67 and Table S4†). In contrast, fluorocages **4** and **7**, similar to **6**, revealed binding affinities well-above $10^6$ $M^{-1}$ (Fig. S64 and S66,† respectively). Note that **5** displayed no binding of $[MeSO_3]^-$ in $CDCl_3$ (Fig. S65†). To our surprise, NMR experiments in the much more polar solvent DMSO ($\varepsilon_r = 46.8$) display **4–7** strongly binding $[MeSO_3]^-$, even when the solution is heated to 100 °C (*in situ* $^1$H NMR, Fig. 2b and Fig. S68–S71†). This finding led us to conclude that binding of $[MeSO_3]^-$ to hosts **4–7** in DMSO-$d_6$ exceeds $K_a$ of $10^6$ $M^{-1}$. Assuming the general anion binding in solution model put forward by Flood *et al.*[59] holds true for $[MeSO_3]^-$, we expect $K_a$ for $[MeSO_3]^-$ binding to hosts **4–7** in $CDCl_3$ to surpass $10^6$ $M^{-1}$ by several orders of magnitude. We note that binding is mostly driven by interaction with the four electropositive H atoms in $C_{Ar}$–H and not by C–H···π

Table 2 Anion association constants ($K_a$, $M^{-1}$) of [*n*-$Bu_4N$][anion] to fluorocage **6**. Thermochemical radii ($r$) in parenthesis

| Host | Solvent | $I^-/Br^-$ | $[N_3]^-$/ $[SCN]^-$ | $[NO_2]^-$/ $[NO_3]^-$ | $[BF_4]^-$ (2.05) | $[HSO_4]^-$ (2.21) | $[ClO_4]^-$ (2.25)/ $[ReO_4]^-$ (2.27) | $[IO_4]^-$ (2.31) | $[PF_6]^-$ (2.42)/ $[SbF_6]^-$ (2.52) | $[MeCO_2]^-$/ $[MeSO_3]^-$ | $[p\text{TsO}]^-$[a] |
|---|---|---|---|---|---|---|---|---|---|---|---|
| **6** | $CDCl_3$ | 161(19)/0 | 8(6)/ 290(8) | 40(40)/ 76(6) | 990(23) | $7(3) \times 10^4$ | $7.91(9) \times 10^3$/ $1.08(2) \times 10^3$ | $1.00(3) \times 10^3$ | $1.510(1) \times 10^4$/ 230(20) | $4.8(3) \times 10^3$/ $>10^6$ | $1.88(4) \times 10^3$ |

[a] *p*Ts = *p*-toluenesulfonyl.

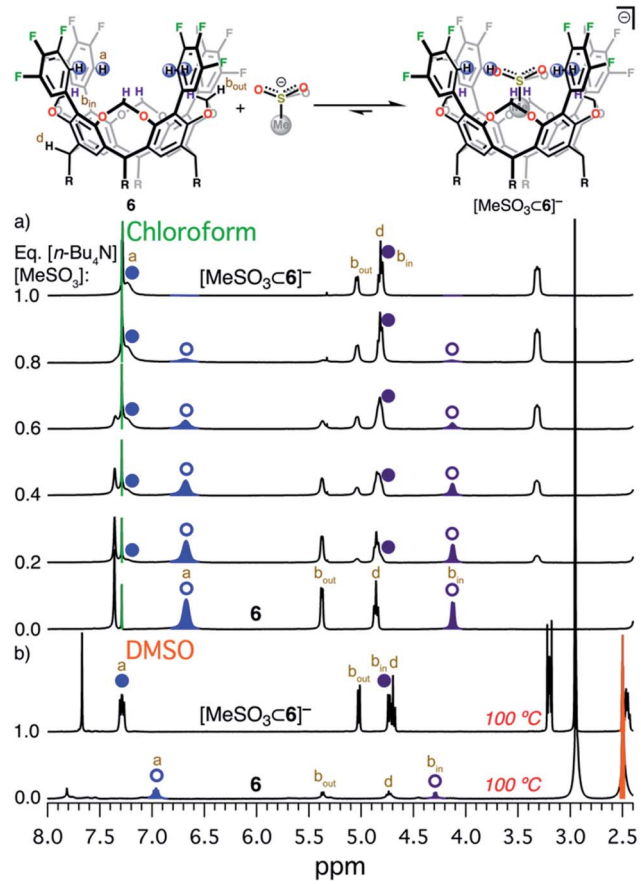


Fig. 2 Equilibrium between **6** and $[MeSO_3]^-$. (a) $^1$H NMR titration of [*n*-$Bu_4N$][$MeSO_3$] into **6** in $CDCl_3$ at 20 °C. (b) $^1$H NMR of **6** (bottom)[55] and [*n*-$Bu_4N$][$MeSO_3\subset$**6**] (top) in DMSO-$d_6$ at 100 °C. Circular symbols correspond to the blue and dark purple hydrogen atoms in the scheme above. Open symbols indicate free host **6**, while solid symbols correspond to the adduct [*n*-$Bu_4N$][$MeSO_3\subset$**6**]. Relevant H atoms are labeled a, $b_{in}$, and $b_{out}$.

interactions found between the Me group in $MeSO_3^-$ and the π system centroids within the resorcin[4]arene backbone since the average C-to-π distance for $[MeSO_3\subset host]^-$, where host = **4**, and **6–8**, is 3.62(3) Å; which is larger than that found in the neutral adduct [MeCN⊂host], for host = **1–6**, and **8** (*vide supra*). Altogether, the qualitative picture portrayed by this NMR data reveals that the equilibrium between host + $[MeSO_3]^-$ and $[MeSO_3\subset host]^-$, for hosts **4–7**, is strongly displaced towards the host–guest adduct.

The strong interaction with methanesulfonate allowed us to isolate and crystallize the adducts [*n*-$Bu_4N$][$MeSO_3\subset$host], for host = **4**, and **6–8** (Fig. S9–S12†). Shown in Fig. 3a is the molecular structure and relevant distances for $[MeSO_3\subset$**6**$]^-$. Note how the three O atoms from the sulfonate group reside in the square plane described by the four electropositive H1X atoms, X = A–D (colored in blue in Scheme 1). This sulfonate anion accommodation maximizes the $C_{Ar}$–H···$O_{MeSO_3^-}$ hydrogen bonding, with remarkably short C-to-O average distances of 3.31(4), 3.24(3), 3.18(7), and 3.34(6) Å for **4**, **6**, **7**, and **8** (Fig. 3b), respectively.[60] Note that the sum of the van der Waals radius for C and O is 3.22 Å.[61] Fluorocages adopt a cone-shaped structure; to determine the expansion of this cone, we measured the distances between rigid carbon atoms C6X (Fig. 3a), X = A–D, which define an almost ideal square (C–$C_{square}$). Plotting these data together, we observe a V-shaped trend in the C-to-O distance, with **7** at the minimum, and no discernible correlation in C–$C_{square}$ distances (Fig. 3b), meaning that strengthening of the hydrogen bonds within the host's cavity only requires rotational movement of the aromatic flanking units as opposed to a breathing in or out distortion.

## DFT-supported structure–function relationship

To gain insight into the trends observed in this family of fluorocages, we performed DFT calculations (M06-2X/6-31+G(d,p) level of theory) in **1–8** to obtain their Hirshfeld Charges (HCs) in

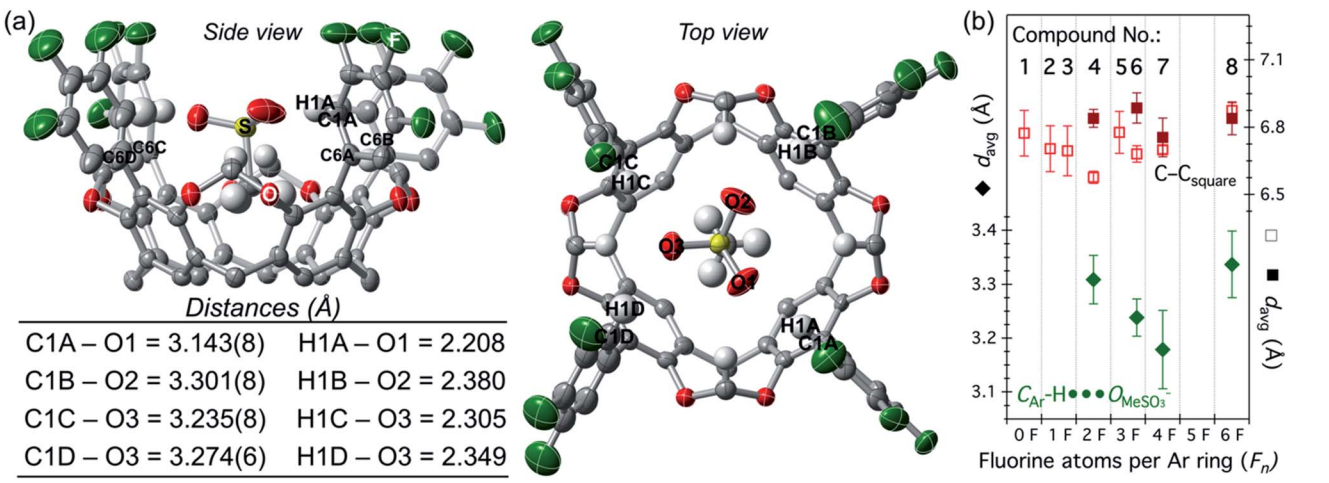


Fig. 3 (a) Side and top view of the molecular crystal structure of $[MeSO_3\subset$**6**$]^-$ obtained at 220 K. Thermal ellipsoids are set at 50% probability level. The $[n\text{-}Bu_4N]^+$, R groups (*n*-pentyl), and H atoms are omitted for clarity, except those H atoms within the inner cavity. (b) Comparison of structural molecular metrics. Average C–$C_{square}$ (red and maroon) and C···O (green) distances. Open symbols correspond to **1–8**, and filled symbols to $[MeSO_3\subset host]^-$, for host = **4**, and **6–8**.

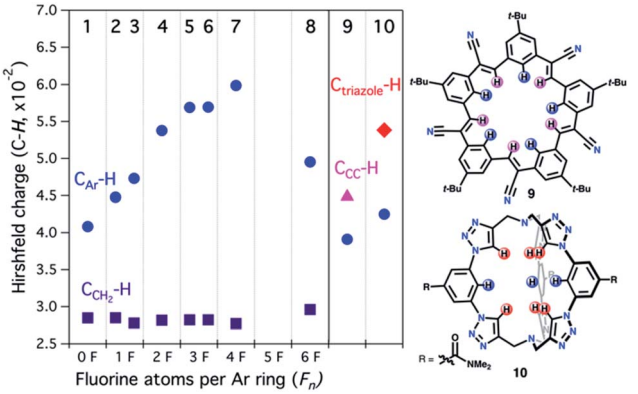


Fig. 4 DFT-calculated Hirshfeld charges for **1–10** (M06-2X/6-31+G(d,p) level of theory). Blue $C_{Ar}$–H, dark purple $C_{CH_2}$–H, pink $C_{CC}$–H, and red $C_{triazole}$–H hydrogen atoms correspond to those shown in Scheme 1 or in the chemdraw drawings in this figure.

an effort to access quantitative data about the electropositivity of the H atoms involved in hydrogen bonding (Fig. 4). Note that HCs are recommended as they yield chemically meaningful partial charges.[62] Following the series from **1** to **7**, we observe a monotonic increase in HC at the H atoms in $C_{Ar}$–H (blue). Unexpectedly, the calculated HCs for fluorocage **8** reside in between those of **3** and **4**. Notably, HCs for **8** explain its weaker binding of $[MeSO_3]^-$ compared to **4–7**. The HC values for the hydrogen atoms in $C_{CH2}$–H (dark purple) are provided in Fig. 4 as control since these should not be affected by the nature of the EWG in the aromatic flanking unit. Overall, this trend correlates well with the binding affinity studies of **1–8**, and with the metrics observed in the host-guest adducts $[n\text{-}Bu_4N][MeSO_3 \subset host]$, for host = **4**, and **6–8** (Fig. 3b). Note that the HCs on **5** and **7** does not correlate well with their binding properties, which we attribute to the conformational distribution observed in the as-synthesized hosts and the large aromatic flanking unit rotational barrier (biaryl bond) of ~22 kcal mol$^{-1}$, compared to ~12 kcal mol$^{-1}$ for all other hosts (Table S5†).

In an effort to compare hosting capabilities of fluorocages with other rigid anion-binding hosts operating solely by C–H hydrogen bonding, we analyzed two recent macrocyclic hosts reported in the literature (Fig. S72†): (1) pentagonal cyanostar **9**, capable of forming a strong 2 : 1 host : guest adduct with $Cl^-$ (40% MeOH/$CDCl_3$, $\beta_2 \approx 10^8$ M$^{-2}$);[22] and (2) cryptand-like triazole cage **10**,[63] which binds $Cl^-$ remarkably strong ($CDCl_3$, $K_a \approx 10^{17}$ M$^{-1}$).[25] HCs of the H atoms involved in C–H hydrogen bonding increase from **9** to **10**, as shown in Fig. 4, supporting the relative trend observed in their anion binding properties. Furthermore, in the case of **10**, the most electropositive H atoms reside in $C_{triazole}$–H and are on par to those found in fluorocage **4**. However, while **4** has four of these electropositive H atoms, **10** has six of them making its internal cavity more electropositive. Most importantly, **5–7** display higher HCs relative to **10** suggesting that further exploration of these fluorocages have the potential to uncover strong affinities for anions of appropriate size to fit in the square planar geometry defined by the blue electropositive H atoms.

## Conclusions

Herein we describe a family of anion hosts – termed fluorocages – sharing the same overall structure, however with anion affinities tuned by several orders of magnitude through a straightforward single four-fold Suzuki–Miyaura cross-coupling synthetic step. These fluorocages are able to bind nonspherical anions, such as sulfonate groups, which display remarkable affinity and size complementarity to their cavity. Further development of this general strategy, and based on the structure–function relationship reported herein, will guide the development of novel, more potent, and selective hosts for anion sequestration from polluted ecosystems, *e.g.*, sulfonate-based PFAS,[64–66] currently an unmet pressing challenge.

## Data availability

All the data have been included in the ESI.†

## Author contributions

S. M. and V. M. E. C. performed the synthesis, titrations, and measurements; S. M. performed the DFT analysis; S. M. and R. H. S. carried out the crystallographic studies; S. M. and R. H. S. conceived the research hypothesis; R. H. S. prepared the manuscript; all authors edited the manuscript.

## Conflicts of interest

There are no conflicts to declare.

## Acknowledgements

We thank the support from the Center for Research Computing and startup funds from the University of Pittsburgh. S. M. acknowledges the support from the Dietrich School of Arts & Sciences Graduate Fellowship and the Andrew Mellon Predoctoral Fellowship.

## Notes and references

1 J. J. Rebek, *Chem. Commun.*, 2000, 637–643.
2 M. Xue, Y. Yang, X. Chi, Z. Zhang and F. Huang, *Acc. Chem. Res.*, 2012, **45**, 1294–1308.
3 G.-W. Zhang, P.-F. Li, Z. Meng, H.-X. Wang, Y. Han and C.-F. Chen, *Angew. Chem., Int. Ed.*, 2016, **55**, 5304–5308.
4 C.-F. Chen and Y. Han, *Acc. Chem. Res.*, 2018, **51**, 2093–2106.
5 L. Escobar and P. Ballester, *Chem. Rev.*, 2021, **121**, 2445–2514.
6 C. Gropp, B. L. Quigley and F. Diederich, *J. Am. Chem. Soc.*, 2018, **140**, 2705–2717.
7 J. Řezáč and P. Hobza, *Chem. Rev.*, 2016, **116**, 5038–5071.
8 A. L. Allred, *J. Inorg. Nucl. Chem.*, 1961, **17**, 215–221.
9 E. Graf and J. M. Lehn, *J. Am. Chem. Soc.*, 1976, **98**, 6403–6405.

10 B. Dietrich, B. Dilworth, J.-M. Lehn, J.-P. Souchez, M. Cesario, J. Guilhem and C. Pascard, *Helv. Chim. Acta*, 1996, **79**, 569–587.
11 K. Bowman-James, *Acc. Chem. Res.*, 2005, **38**, 671–678.
12 W. B. Farnham, D. C. Roe, D. A. Dixon, J. C. Calabrese and R. L. Harlow, *J. Am. Chem. Soc.*, 1990, **112**, 7707–7718.
13 O. B. Berryman, A. C. Sather, B. P. Hay, J. S. Meisner and D. W. Johnson, *J. Am. Chem. Soc.*, 2008, **130**, 10895–10897.
14 J. Cai and J. L. Sessler, *Chem. Soc. Rev.*, 2014, **43**, 6198–6213.
15 P. A. Gale, J. L. Sessler, V. Kral and V. Lynch, *J. Am. Chem. Soc.*, 1996, **118**, 5140–5141.
16 C.-H. Lee, H.-K. Na, D.-W. Yoon, D.-H. Won, W.-S. Cho, V. M. Lynch, S. V. Shevchuk and J. L. Sessler, *J. Am. Chem. Soc.*, 2003, **125**, 7301–7306.
17 D.-W. Yoon, D. E. Gross, V. M. Lynch, J. L. Sessler, B. P. Hay and C.-H. Lee, *Angew. Chem., Int. Ed.*, 2008, **47**, 5038–5042.
18 S. J. Edwards, H. Valkenier, N. Busschaert, P. A. Gale and A. P. Davis, *Angew. Chem., Int. Ed.*, 2015, **54**, 4592–4596.
19 A. J. Ayling, M. N. Pérez-Payán and A. P. Davis, *J. Am. Chem. Soc.*, 2001, **123**, 12716–12717.
20 J. P. Clare, A. J. Ayling, J.-B. Joos, A. L. Sisson, G. Magro, M. N. Pérez-Payán, T. N. Lambert, R. Shukla, B. D. Smith and A. P. Davis, *J. Am. Chem. Soc.*, 2005, **127**, 10739–10746.
21 Y. Li and A. H. Flood, *Angew. Chem., Int. Ed.*, 2008, **47**, 2649–2652.
22 S. Lee, C.-H. Chen and A. H. Flood, *Nat. Chem.*, 2013, **5**, 704–710.
23 S. Lee, B. E. Hirsch, Y. Liu, J. R. Dobscha, D. W. Burke, S. L. Tait and A. H. Flood, *Chem. - Eur. J.*, 2016, **22**, 560–569.
24 F. C. Parks, Y. Liu, S. Debnath, S. R. Stutsman, K. Raghavachari and A. H. Flood, *J. Am. Chem. Soc.*, 2018, **140**, 17711–17723.
25 Y. Liu, W. Zhao, C.-H. Chen and A. H. Flood, *Science*, 2019, **365**, 159.
26 J. Svec, M. Necas and V. Sindelar, *Angew. Chem., Int. Ed.*, 2010, **49**, 2378–2381.
27 T. Lizal and V. Sindelar, *Isr. J. Chem.*, 2018, **58**, 326–333.
28 N. R. Song, J. H. Moon, J. Choi, E. J. Jun, Y. Kim, S.-J. Kim, J. Y. Lee and J. Yoon, *Chem. Sci.*, 2013, **4**, 1765–1771.
29 H. Zhou, Y. Zhao, G. Gao, S. Li, J. Lan and J. You, *J. Am. Chem. Soc.*, 2013, **135**, 14908–14911.
30 M. Lisbjerg, H. Valkenier, B. M. Jessen, H. Al-Kerdi, A. P. Davis and M. Pittelkow, *J. Am. Chem. Soc.*, 2015, **137**, 4948–4951.
31 J. Shang, W. Zhao, X. Li, Y. Wang and H. Jiang, *Chem. Commun.*, 2016, **52**, 4505–4508.
32 H. Gregolińska, M. Majewski, P. J. Chmielewski, J. Gregoliński, A. Chien, J. Zhou, Y.-L. Wu, Y. J. Bae, M. R. Wasielewski, P. M. Zimmerman and M. Stępień, *J. Am. Chem. Soc.*, 2018, **140**, 14474–14480.
33 L. M. Eytel, H. A. Fargher, M. M. Haley and D. W. Johnson, *Chem. Commun.*, 2019, **55**, 5195–5206.
34 H.-Y. Gong, B. M. Rambo, E. Karnas, V. M. Lynch and J. L. Sessler, *Nat. Chem.*, 2010, **2**, 406–409.
35 N. Lopez, D. J. Graham, R. McGuire, G. E. Alliger, Y. Shao-Horn, C. C. Cummins and D. G. Nocera, *Science*, 2012, **335**, 450.
36 E. M. Fatila, E. B. Twum, A. Sengupta, M. Pink, J. A. Karty, K. Raghavachari and A. H. Flood, *Angew. Chem., Int. Ed.*, 2016, **55**, 14057–14062.
37 B. Qiao, G. M. Leverick, W. Zhao, A. H. Flood, J. A. Johnson and Y. Shao-Horn, *J. Am. Chem. Soc.*, 2018, **140**, 10932–10936.
38 R. O. Ramabhadran, Y. Liu, Y. Hua, M. Ciardi, A. H. Flood and K. Raghavachari, *J. Am. Chem. Soc.*, 2014, **136**, 5078–5089.
39 W. Zhao, B. Qiao, C.-H. Chen and A. H. Flood, *Angew. Chem., Int. Ed.*, 2017, **56**, 13083–13087.
40 S. K. Kim, B.-G. Kang, H. S. Koh, Y. J. Yoon, S. J. Jung, B. Jeong, K.-D. Lee and J. Yoon, *Org. Lett.*, 2004, **6**, 4655–4658.
41 J. Y. Kwon, N. J. Singh, H. N. Kim, S. K. Kim, K. S. Kim and J. Yoon, *J. Am. Chem. Soc.*, 2004, **126**, 8892–8893.
42 M. Arunachalam and P. Ghosh, *Inorg. Chem.*, 2010, **49**, 943–951.
43 S.-Y. Zhuang, Y. Cheng, Q. Zhang, S. Tong and M.-X. Wang, *Angew. Chem., Int. Ed.*, 2020, **59**, 23716–23723.
44 H. Xie, T. J. Finnegan, V. W. Liyana Gunawardana, R. Z. Pavlović, C. E. Moore and J. D. Badjić, *J. Am. Chem. Soc.*, 2021, **143**, 3874–3880.
45 P. Timmerman, W. Verboom and D. N. Reinhoudt, *Tetrahedron*, 1996, **52**, 2663–2704.
46 O. Hayashida, A. Shivanyuk and J. J. Rebek, *Angew. Chem., Int. Ed.*, 2002, **41**, 3423–3426.
47 S. S. Zhu, H. Staats, K. Brandhorst, J. Grunenberg, F. Gruppi, E. Dalcanale, A. Lützen, K. Rissanen and C. A. Schalley, *Angew. Chem., Int. Ed.*, 2008, **47**, 788–792.
48 J. A. Bryant, M. T. Blanda, M. Vincenti and D. J. Cram, *J. Am. Chem. Soc.*, 1991, **113**, 2167–2172.
49 C. B. Aakeröy, P. D. Chopade, N. Schultheiss and J. Desper, *Eur. J. Org. Chem.*, 2011, **2011**, 6789–6793.
50 D. H. Williams and M. S. Westwell, *Chem. Soc. Rev.*, 1998, **27**, 57–64.
51 K. N. Houk, A. G. Leach, S. P. Kim and X. Zhang, *Angew. Chem., Int. Ed.*, 2003, **42**, 4872–4897.
52 P. Thordarson, *Chem. Soc. Rev.*, 2011, **40**, 1305–1323.
53 B. Qiao, J. R. Anderson, M. Pink and A. H. Flood, *Chem. Commun.*, 2016, **52**, 8683–8686.
54 H. K. Roobottom, H. D. B. Jenkins, J. Passmore and L. Glasser, *J. Chem. Educ.*, 1999, **76**, 1570.
55 *Host **6** has extremely low solubility in DMSO, even at 100 °C.*
56 K. Choi and A. D. Hamilton, *J. Am. Chem. Soc.*, 2003, **125**, 10241–10249.
57 M. B. Nielsen, J. O. Jeppesen, J. Lau, C. Lomholt, D. Damgaard, J. P. Jacobsen, J. Becher and J. F. Stoddart, *J. Org. Chem.*, 2001, **66**, 3559–3563.
58 The exchange barrier for anion binding likely results from steric impediment of the $CF_3$ groups in 8, as shown in Fig. S12.†.
59 Y. Liu, A. Sengupta, K. Raghavachari and A. H. Flood, *Chem*, 2017, **3**, 411–427.
60 *The H-to-O distance comprising formally the hydrogen bonds seen here are remarkably short. However, since the H atoms are not refined (they are simply fixed to the structure through*

*AFIX commands), we decided not to relay on those figures and instead use the more reliable C-to-O distances*.

61 A. Bondi, *J. Phys. Chem.*, 1964, **68**, 441–451.

62 C. Fonseca Guerra, J.-W. Handgraaf, E. J. Baerends and F. M. Bickelhaupt, *J. Comput. Chem.*, 2004, **25**, 189–210.

63 *Host **10** has been reported with R = –CONCy$_2$, however to reduce computational costs, Cy was truncated to Me*.

64 C. F. Kwiatkowski, D. Q. Andrews, L. S. Birnbaum, T. A. Bruton, J. C. DeWitt, D. R. U. Knappe, M. V. Maffini, M. F. Miller, K. E. Pelch, A. Reade, A. Soehl, X. Trier, M. Venier, C. C. Wagner, Z. Wang and A. Blum, *Environ. Sci. Technol. Lett.*, 2020, **7**, 532–543.

65 D. Q. Andrews and O. V. Naidenko, *Environ. Sci. Technol. Lett.*, 2020, **7**, 931–936.

66 A. Bălan Simona, C. Mathrani Vivek, F. Guo Dennis and M. Algazi André, *Environ. Health Perspect.*, 2021, **129**, 025001.